Engineering Science and Technology, an International Journal 79 (2026) 102422

Contents lists available at ScienceDirect

Engineering Science and Technology, an International Journal

journal homepage: www.elsevier.com/locate/jestch

Microstructural and mechanical enhancement of AA2024 via multi-pass friction stir processing with HEA (FeNiCrAlCu) particle reinforcement

Harun Yanar [a], Dursun Murat Sekban [b,c], Serdar Ozkaya [d], Abdullah Hasan Karabacak [d], Semih Mahmut Aktarer [e], Abdulkadir Coskun [b], Abdelouahed Tounsi [f,g], Murat Yaylacı [h,ı,*]

[a] Karadeniz Technical University, Mechanical Engineering, Trabzon 61080, Turkey
[b] Karadeniz Technical University, Department of Marine Engineering Operations, 61080 Trabzon, Turkey
[c] Trabzon Teknokent, WMS Engineering Services Industry Trade Limited Company, 61080 Trabzon, Turkey
[d] Karadeniz Technical University, Metallurgical and Materials Engineering, 61080 Trabzon, Turkey
[e] Recep Tayyip Erdogan University, Department of Automotive Technology, 53020 Rize, Turkey
[f] Department of Civil and Environmental Engineering, King Fahd University of Petroleum & Minerals, 31261 Dhahran, Eastern Province, Saudi Arabia
[g] Material and Hydrology Laboratory, University of Sidi Bel Abbes, Faculty of Technology, Civil Engineering Department, Algeria
[h] Department of Civil Engineering, Recep Tayyip Erdogan University, 53100 Rize, Türkiye
[ı] Faculty of Turgut Kıran Maritime, Recep Tayyip Erdogan University, 53900 Rize, Türkiye

ARTICLE INFO

Keywords:
Friction stir process
Metal matrix composites
High entropy alloy
AA2024

ABSTRACT

Friction stir processing (FSP) is an effective solid-state technique for fabricating aluminum-based metal matrix composites (MMCs) with refined and homogeneous microstructures. In this study, HEA (FeNiCrAlCu) powders were incorporated into AA2024 aluminum alloy via multi-pass FSP using 1, 2, and 3-passes. The effects of pass number on microstructural evolution, mechanical properties, tribological behavior, and corrosion resistance were investigated using SEM, XRD, hardness, tensile, wear, and electrochemical corrosion tests. Increasing the FSP pass number promoted progressive fragmentation and more uniform dispersion of HEA particles, as supported by SEM observations and ImageJ-based measurements, resulting in a more homogeneous composite structure. This microstructural improvement directly enhanced the mechanical, wear, and corrosion performance of the composites. For the 3-pass FSPed composite, hardness increased from 155 to 258 HBN, tensile strength from 188 to 246 MPa, and uniform elongation from 3.0 ± 0.5 to 3.6 ± 0.3 mm compared with the base AA2024 alloy. In addition, corrosion current density decreased from 6.94 to 1.36 μA, corrosion potential shifted from − 703 to − 548 mV, and corrosion rate decreased from 14.79 to 3.11 mpy. The 3-pass FSPed composite also exhibited the lowest volumetric wear rate and a more stable friction response.

1. Introduction

AA 2024 series aluminum alloys are alloys that contain copper and are frequently used in the aviation sector due to their relatively high strength and fatigue properties. Although these alloys are often used by methods such as rolling or extrusion after casting, it has been observed that the use of this alloy as a matrix material and the use of various reinforcement elements by converting it into a metal matrix composite (MMC) has increased rapidly in recent years [1–17]. On the other hand, when the reinforcement elements used in MMCs are examined, it is known that the use of high entropy alloy (HEA) has increased in recent years due to the advantages it provides to the structure in terms of hardness, strength and corrosion resistance [18–22]. Recent studies have also emphasized HEA particles as promising multifunctional reinforcements for aluminum based MMCs, particularly due to their combined strengthening and corrosion resistance potential [23–25].

Although various methods are used to form MMCs, friction stir process (FSP) has become a method frequently used in the formation of MMC due to its various advantages. The basic advantages of FSP in the production of MMC are the ability to obtain a homogeneous internal structure after the process, the relatively low heat and energy inputs required during the process, its application to plate type materials and the relative reduction of porosity in the structure. The FSP method is a severe plastic deformation (SPD) method based on the basic application principle of friction stir welding (FSW) [26–30]. In this method, processing parameters such as tool rotation speed, traverse speed, axial

* Corresponding author at: Department of Civil Engineering, Recep Tayyip Erdogan University, 53100 Rize, Türkiye.
E-mail address: murat.yaylaci@erdogan.edu.tr (M. Yaylacı).

https://doi.org/10.1016/j.jestch.2026.102422
Received 12 February 2026; Received in revised form 29 April 2026; Accepted 25 May 2026
Available online 29 May 2026

force, and the number of passes directly affect material flow, heat input, and reinforcement distribution. It is known that quite successful results are obtained for the development of microstructure and mechanical properties for many different material groups with FSP [31–42]. In recent years, studies on the incorporation of reinforcement powders into machined grooves on aluminum plates by FSP have increased rapidly [43–47]. In this regard, the number of FSP passes is considered a critical parameter controlling the microstructural evolution of MMCs [48–50]. Recent multi-pass FSP studies have shown that repeated passes can improve reinforcement fragmentation, particle dispersion, and stir-zone homogeneity in aluminum-based MMCs, leading to improved mechanical and wear properties [48–54]. However, these studies have mostly focused on ceramic or oxide reinforcements rather than HEA particles.

It is extremely important to reveal the changes in the internal structural and mechanical properties of the MMC formed by adding HEA reinforcement to the AA2024 alloy in order to diversify the industrial uses of AA2024 alloys. Therefore, the novelty of the present study lies in the fabrication of AA2024/HEA MMCs via multi-pass friction stir processing and the systematic evaluation of the effect of pass number on microstructural evolution, mechanical performance, tribological behavior, and corrosion resistance. However, despite the growing interest in both HEA-reinforced aluminum matrix composites and multi-pass FSP, the pass-number-dependent fabrication and performance evaluation of AA2024/FeNiCrAlCu HEA composites by FSP remain insufficiently addressed in the literature. In this context, in this study, AA2024/HEA MMCs were formed by adding HEA reinforcement to the AA2024 matrix material using FSP in varying pass numbers (1 pass, 2 passes and 3 passes), and then the changes in the microstructural and mechanical properties of the base material and MMCs were examined in detail. As a result of the examinations, it was determined that the HEA reinforcement was distributed much more homogeneously in the matrix AA2024 with the increasing number of passes. It was determined that hardness, strength and corrosion resistance improved in all MMCs formed according to the base AA2024 alloy, and the highest values were reached within the MMCs after 3-passes of FSP. On the other hand, it was observed that the wear resistance improved after the formation of MMC with FSP, and this improvement in wear increased with the homogeneous distribution of the reinforcement element depending on the increasing number of passes.

2. Experimental procedure

2.1. MMC sample preparation process

High-entropy alloys (HEAs) designed with equimolar ratios facilitate the formation of stable solid solution phases due to their high configurational entropy and, at the same time, limit the formation of brittle and undesirable intermediate phases [55]. These structural advantages are particularly important in the production of MMCs using solid-state processing methods such as friction stirring, as phase stability and homogeneous distribution of the reinforcement phase within the matrix directly affect the final mechanical performance. However, in systems containing more than five elements, the increased number of components can lead to disadvantages such as phase complexity, segregation tendencies, and processability problems during the production process [56]. Therefore, in this study, five-component equimolar ratio HEA powders were preferred to provide both phase stability advantages and ease of processing. The selection of Fe, Ni, Al, Cu, and Cr as the constituent elements of the HEA was based on their complementary contributions to the alloy system. Fe and Cr enhance mechanical strength and provide resistance against oxidation, while Ni improves toughness and contributes to the thermal and mechanical stability of the composite. Al, due to its low density and high compatibility with aluminum matrices, reduces the overall weight and promotes favorable diffusion behavior. Cu supports both electrical and thermal conductivity, further improving the multifunctional characteristics of the composite. The combination of these elements increases the configurational entropy of the system, encouraging the formation of stable solid-solution phases and ensuring a balanced improvement in mechanical and corrosion performance. The HEA powders used in this study consisted of equimolar amounts of Fe, Ni, Al, Cu, and Cr, corresponding to 20 at.% for each element.

The experimental process of this study began with the preparation of HEA powders, which were then incorporated into an Al alloy matrix using a friction stir process (FSP) to produce MMCs. Microstructural examinations and mechanical tests were performed on the produced samples, and the resulting data were graphically analyzed and interpreted. All of these steps are schematically illustrated in Fig. 1.

The HEA powders in this study were made by mechanical alloying in a Fritsch Pulverisette 7 planetary ball mill. Tungsten carbide milling balls with a diameter of 10 mm were put into the milling chamber with the elemental powders, and the procedure was carried out under an argon-protected environment at a rotational speed of 400 rpm. A ball-to-powder weight ratio of 5:1 was used, and the milling time was 25 h. To minimize overheating, oxidation, and cold welding during the alloying process, methanol was introduced to the chamber at a 2 wt% concentration as a process control agent. The average particle sizes of the starting Al, Cr, Cu, Fe, and Ni powders used for HEA synthesis were 85.6 μm, 27.8 μm, 69.5 μm, 46.4 μm, and 44.4 μm, respectively. The mechanically alloyed FeNiCrAlCu powder was used as the HEA reinforcement in this study, and its phase-related features after FSP were evaluated based on the XRD and EDS results of the processed composites.

AA2024-T351 alloy plates were used as the matrix material, and HEA powders were incorporated through a groove filling approach. The nominal HEA reinforcement content was approximately 10 wt%, determined based on the powder-filled groove geometry and the processed zone. This reinforcement level was selected as a practical content to provide a detectable strengthening effect while maintaining processability and limiting excessive particle agglomeration during FSP. For this purpose, channels were created along the center section of the AA2024 plates with the recorded dimensions, each with a 1 mm profile and a 2 mm depth as shown in Fig. 2a. These channels were filled with HEA powder. FSP operations were performed using the FSWM 10–400 model machine manufactured by WMS Engineering. During the process, the tool rotation speed was 1000 rpm, the tool feed rate was 40 mm/min, and the axial force was 1100 kg. These parameters were selected to ensure sufficient material flow and HEA particle incorporation while limiting excessive heat input, flash formation, and particle loss from the stir zone. The tool used for FSP was made of tungsten carbide and had a shoulder diameter of 18 mm, a tip diameter of 8 mm, and a tip length of 3.8 mm. The tool had a cylindrical pin geometry, and an M5 metric thread was machined on the pin surface to enhance material flow and promote the dispersion of HEA powders within the AA2024 matrix. All FSP passes were applied in the same processing direction. To ensure microstructural homogeneity and its effects on material properties, FSP was designed in 1, 2, and 3 passes. Under this fixed processing window, the effect of pass number was isolated, and the repeated passes increased cumulative stirring and plastic deformation without changing the basic heat input condition. In the present study, three passes were selected as a practical upper limit to evaluate the effect of repeated FSP while avoiding excessive processing time, cumulative heat input, and possible tool wear associated with higher pass numbers.

2.2. Microstructure and mechanical properties

The sampling locations and prepared specimens for microstructure, hardness, wear, tensile and corrosion tests are schematically shown in Fig. 2b. The microstructures of MMCs were analyzed using a Zeiss Evo LS10 scanning electron microscope (SEM). The MMCs were analyzed using X-ray diffraction (XRD) at 45 kV and 40 mA with Cu K(alpha) radiation (1.541874 Å). XRD patterns were obtained in the 2θ region of

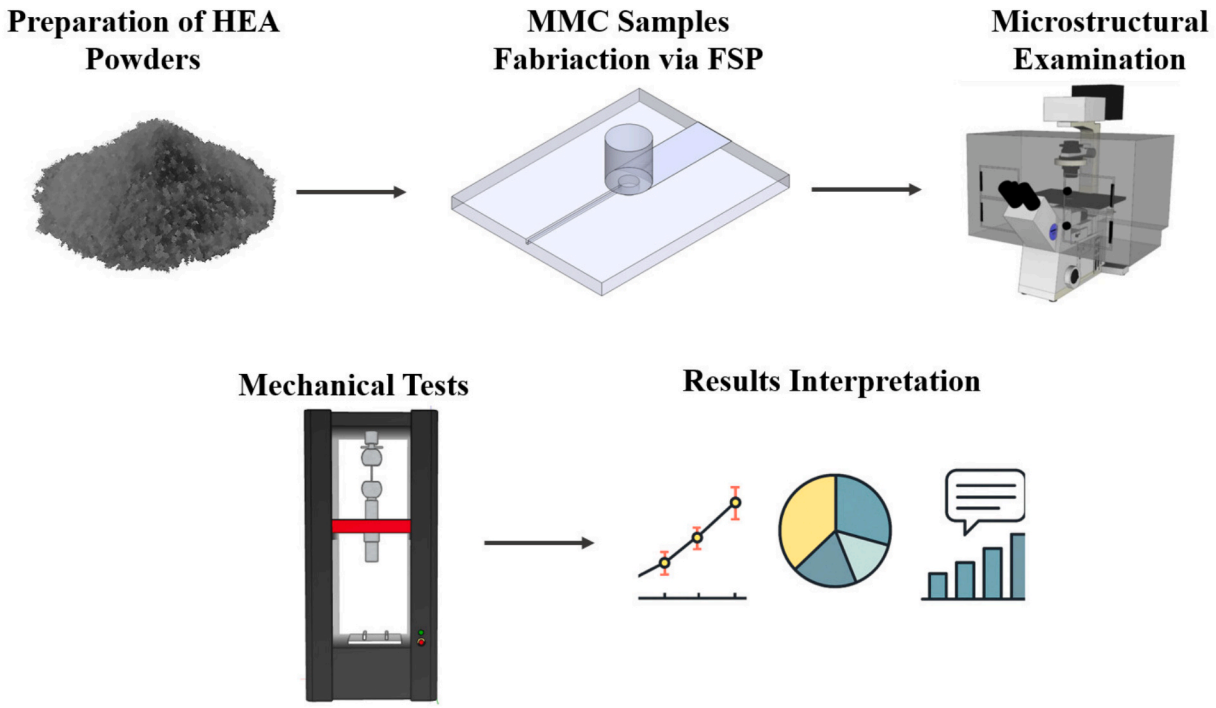

Fig. 1. Schematic illustration of the work steps.

35-90° using a one-second time step and 0.01° step size. The ImageJ software was used to do quantitative measurements. The linear intercept technique was used to measure grain size, while histogram thresholding was used to determine phase fractions. XRD peaks were used to measure the crystallite size of AA2024 using the Debye-Scherrer method. Furthermore, as the number of passes increased, crystallite size (D_P), microstrain (ε), dislocation density (δ), and D-spacing values were also measured.

$D_P = \frac{0.94\lambda}{\beta cos\theta}$ Eq.1.

where; D_P is the crystallite size, λ is the wavelength ($1.54x10^{-10}$m), β is the diffraction broadening i.e. (FWHM), and θ is the diffraction angle.

$\delta = \frac{1}{D_P{}^2}$ Eq.2.

where; δ = dislocation density.

$\varepsilon = \frac{\beta cos\theta}{4}$ Eq.3.

where; ε = micro strain

Brinell hardness test was applied to determine the hardness values of MMCs formed by applying FSP in the main structure and different pass numbers. For the tests, a 2.5 mm diameter penetrating tip and a 31.25 kgf force were used for 10 s. Hardness measurements were taken from different locations across the FSP stir zone to account for local variations in the processed region. Hardness values were determined by averaging at least three measurements for each condition. The tensile specimens were extracted from the processed region and tested at room temperature with a deformation rate of 5×10^{-4} s^{-1} using an Instron 3382 universal tensile compression tester. The specimens were prepared in accordance with ASTM E8/E8M, with a reduced-section cross-section of 2 mm × 3 mm and a gauge length of 26 mm. Tensile tests were repeated at least three times for each condition, and the values reported in Table 2 are presented as mean ± standard deviation.

Wear tests on AA2024-HEA MMC samples were performed using a ball-on-disc type tribometer (UTS Tribolog, Trabzon, Türkiye) in accordance with the ASTM G133 standard. All wear tests were conducted in ambient air under controlled laboratory conditions at 27 °C and approximately 40% relative humidity. Specimens measuring 20 × 20 × 3 mm^3 were sectioned from the processed samples using Electrical Discharge Machining (EDM). Prior to testing, sample surfaces were sequentially ground with emery papers and polished with a cloth to achieve a surface roughness of approximately 0.1 μm (Ra). The counterface material was a 6 mm diameter AISI 52100 steel ball with a hardness of 60 HRC. All tests were conducted over 5000 reciprocating cycles under a 5 N normal load, with a stroke length of 12 mm and a frequency of 1 Hz. These conditions were selected to provide a reproducible moderate-load dry sliding contact in accordance with ASTM G133 and to compare the relative wear response of the processed samples under identical conditions. Each test condition was repeated at least twice to confirm the consistency of the results. After testing, 2D surface topographies of the wear tracks were obtained using an optical profilometer (Nanofocus μscan, Germany), and worn surfaces were further analyzed via scanning electron microscopy (FESEM, Thermo Fisher). The wear rate (ω) was calculated using the formula ω = V / (F × S), where V represents the volumetric material loss (cm^3), F is the applied normal load (N), and S is the total sliding distance (m).

Corrosion tests were conducted on 18 × 6 × 2 mm samples taken from the main structure and MMC samples. Electrochemical experiments were conducted using the Gamry Reference 3000 device in 3.5% NaCl solution, with an open circuit potential range of ± 500 mV and a scanning speed of 1 mV/s. Corrosion characterisation was assessed using corrosion potential and current density measurements. Each scenario was repeated three times, and the average data was used to construct corrosion curves. The corrosion rate was determined using the current density (Icorr) derived from the Tafel plots, according to the following equation:

$\text{Corrosion Rate (mpy)} = \frac{0.13 \text{ x } I_{corr} \text{ x EW}}{\rho}$ Eq.4.

In this formula, I_{corr} represents the corrosion current density (μA cm^{-2}), EW is the equivalent weight of the metal (g/equiv), ρ denotes the density of the metal (g/cm^3), and 0.13 is a unit conversion factor used to express the result in mpy.

3. Results and discussions

3.1. Microstructure

When the SEM (200 ×) images of the samples treated with 1, 2, and 3 passes, shown in Fig. 3, are examined, significant changes are observed

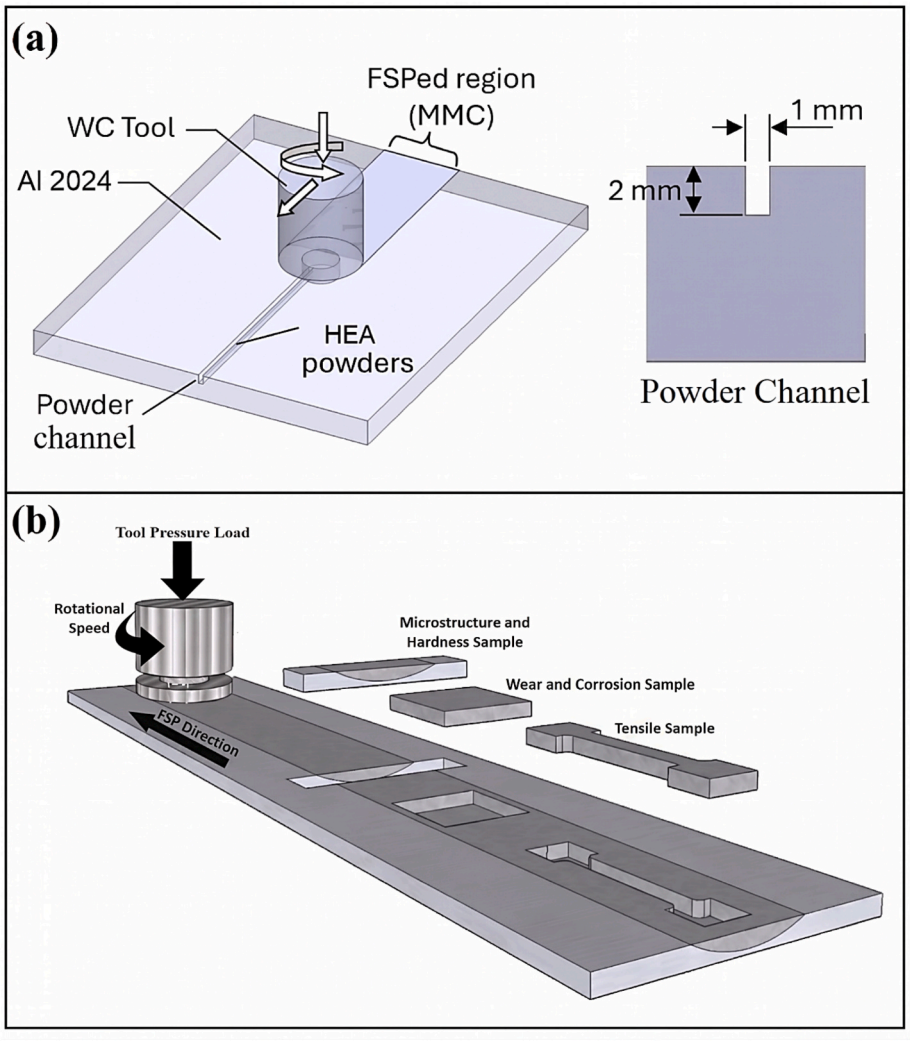

Fig. 2. (a) Schematic view of the powder channel and FSP process; (b) schematic view of the FSP setup and prepared test samples.

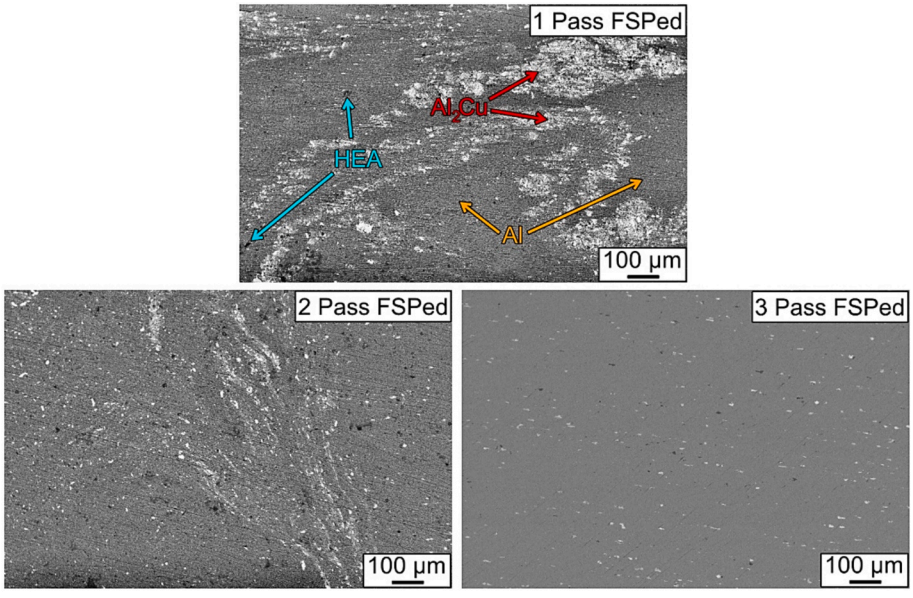

Fig. 3. Microstructure images of composite samples after SEM analysis.

in the morphology and distribution of both the Al_2Cu intermetallic phase and the HEA phase with increasing number of pass. White areas represent the Al_2Cu intermetallics, gray areas represent the Al matrix, and dark gray and black areas represent the HEA intermetallic phase. In addition to qualitative SEM observations, ImageJ-based semi-quantitative measurements were performed on the SEM images to compare the relative Al_2Cu-rich regions and the apparent HEA particle/cluster size in the processed samples. Although this analysis does not represent a full three-dimensional particle-size distribution, it provides comparative evidence for the progressive reduction of coarse HEA-rich regions and Al_2Cu-rich areas with increasing FSP pass number. In the single-pass sample, the Al_2Cu particles are coarse, irregular, and dispersed in the matrix, sometimes clustered. Similarly, the HEA phase is observed as large, sharp-edged regions. This indicates that the mixing and dispersion effect of the single-pass FSP is limited, and in particular, the reinforcement phases and the Al_2Cu intermetallics are not completely broken and homogenized. This also suggests that one pass was not sufficient under the selected FSP parameters to achieve complete reinforcement dispersion. Similar phase clustering and inhomogeneous distribution have been reported in the literature in single-pass FSP applications [57]. A significant change in the microstructure occurred after the second pass. The Al_2Cu particles became finer and more uniform, and large particles were broken and distributed more evenly in the matrix. The dark regions belonging to the HEA phase were also noticeably fragmented and reduced in size. The increased mixing and particle breaking effect with the two-pass application allows both the reinforcement phase and the Al_2Cu to transform into a more homogeneous structure. This improvement is consistent with literature findings that multi-pass FSP breaks up reinforcement phase clusters and provides a more uniform distribution within the matrix [58]. The microstructure obtained after the third pass FSP is the most homogeneous and fine-grained. White Al_2Cu particles are now visible only as very small and fine precipitates, distributed evenly throughout the matrix. The HEA phase is almost completely broken down into small particles, and large agglomerates have disappeared. The matrix structure is much cleaner and more continuous. This demonstrates that repeated FSP is effective in terms of both phase refinement and phase dissolution/homogenization. Rubtsov et al. (2023) [57] reported that multi-pass FSP completely breaks down the Cu-based coarse intermetallics, converting them into a homogeneous distribution. Furthermore, by increasing the amount of Al-Cu intermetallics, the stir zone becomes more uniform.

According to the EDS maps in Fig. 4, the Al matrix, shown as red, is observed as the continuous and dominant phase throughout the microstructure of the sample. This confirms that Al is the main carrier phase in the AA2024 alloy. On the other hand, Cu (yellow), Fe (green), Ni (blue), and Cr (purple) signals are concentrated in distinct particulate

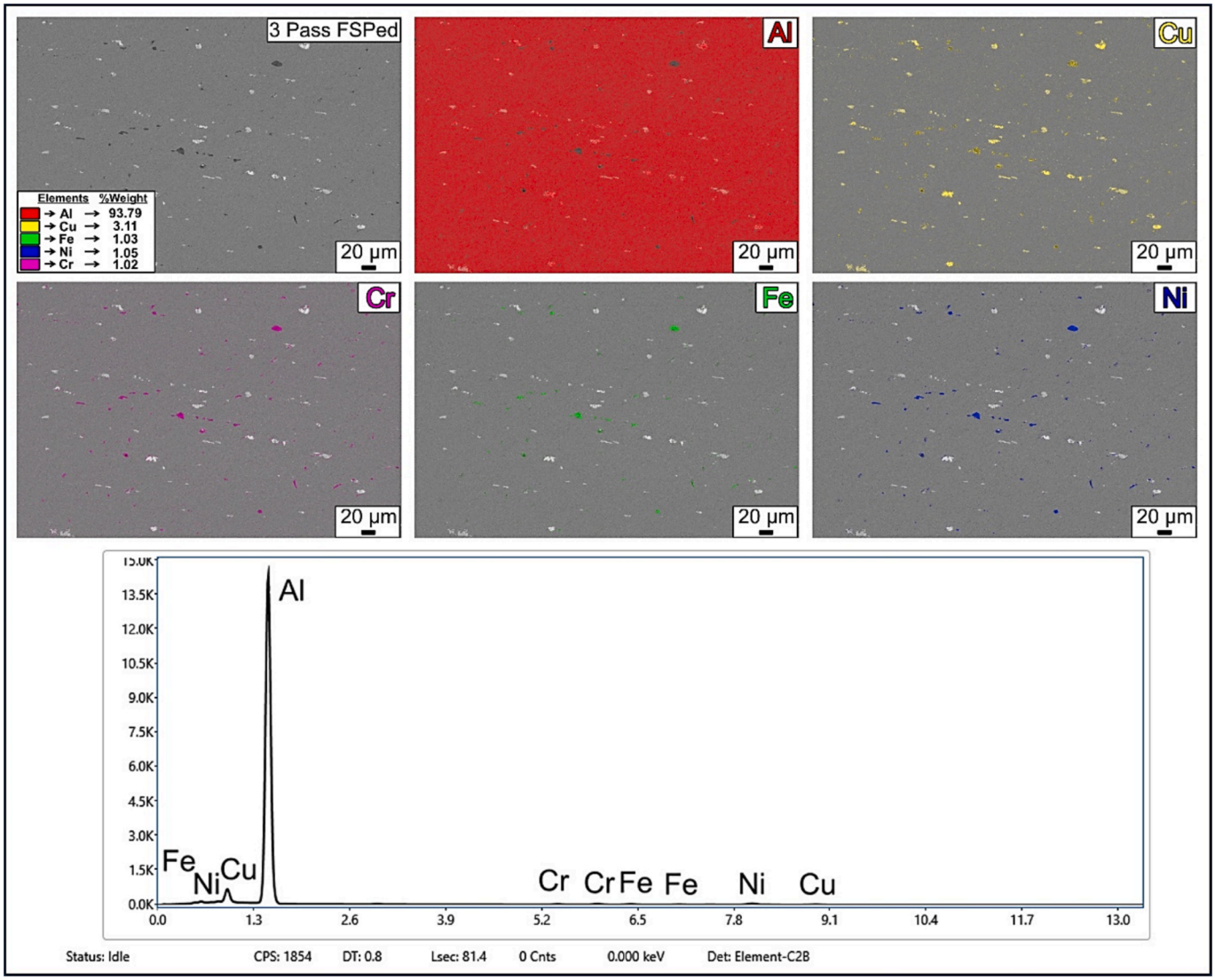

Fig. 4. EDS mapping analysis of the 3-pass FSPed sample.

clusters in the maps. The high-intensity signals of these elements overlap with the areas where HEA reinforcement particles are located. In other words, due to the strong plastic deformation and yielding induced by FSP, HEA particles are finely dispersed within the Al matrix. Similarly, a homogeneous distribution of HEA particles has been reported in the literature in HEA-reinforced FSP composites [59]. The maps show the presence of Cu-Fe-Ni-Cr elements in clusters in the same regions, indicating that the multi-element HEA phase is preserved in the particulate structure. However, the EDS results are used here primarily to demonstrate elemental co-localization and distribution; they should not be interpreted alone as direct crystallographic evidence of HEA phase stability.

The dissolution and segregation trends of these elements in the matrix can also be observed in the analysis. The EDS spectrum does not display the characteristic peak intensities of θ phases, such as Al_2Cu, suggesting that Al-Cu precipitates largely dissolved and incorporated into the matrix during FSP. At the same time, the HEA reinforcement particles maintained their integrated structure after FSP. For example, in the FSP study conducted on CoCrFeNiCu HEA, the initial Cu element segregation almost completely disappeared, and the coarse-grained two-phase structure transformed into an ultrafine-grained single-phase structure [60]. These results indicate that, thanks to the intense mixing effect of FSP and the "slow diffusion" characteristics of HEA, the HEA particles remained structurally stable, and no significant phase separation occurred.

The EDS spectrum in the lower section also confirms these findings: the highest peak is observed for Al, while the Cu, Fe, Ni, and Cr peaks are lower; this verifies the dominant concentration of the Al matrix and is consistent with the spread in the maps. In other words, the peak heights in the spectrum are consistent with the dense regions seen in the elemental maps in Fig. 4. High-magnification SEM/EDS observations also showed that the HEA particles were embedded in the AA2024 matrix without obvious interfacial pores, microcracks, or a continuous brittle reaction layer. This interfacial integrity is important for effective load transfer between the matrix and reinforcement, and it supports the improved hardness, tensile strength, and wear resistance obtained after multi-pass FSP [54,61–63]. These microstructural observations also coincide with the SEM and XRD findings. XRD analyses revealed that the Al_2Cu phase was significantly reduced after FSP, leaving behind phases belonging to the Al matrix and HEA reinforcement. Since the EDS maps of the 3-pass FSPed sample show that the HEA-related elements were distributed within the Al matrix without obvious elemental separation, this supports the microstructural evidence for improved dispersion after repeated FSP.

When Fig. 5 is examined, significant intensity changes are observed in the characteristic peaks of the Al2024 aluminum matrix [38.5° (111), 44.7° (200), 65.1° (220), 78.2° (311), 82.4° (222)] depending on the number of passes. When a single FSP pass (1 pass) is applied, the Al matrix peaks are observed with high intensity, while after multiple passes (2 and 3 passes), the relative intensity distribution of these peaks changes. In particular, the peak belonging to the (111) plane shows one of the highest intensities after the first pass, while a decrease in the relative intensity of this peak is observed with increasing pass number, while the relative intensities of some other peaks (e.g. (220) and (311)) increase. This is related to the crystallographic texture change created in the material by the FSP process; Multiple passes randomize the grain orientation distribution and reduce the preferential orientation toward certain planes, resulting in a more balanced Al peak intensity ratio. Consequently, increasing the number of passes results in a more isotropic character in the XRD pattern of the Al matrix phase.

Similarly, the microstructural parameters listed in Table 1 quantitatively demonstrate the effects of FSP on the number of passes. The XRD-derived crystallite size decreased from approximately 45.22 nm in the 1-pass sample to 14.35 nm in the 3-pass sample, indicating refinement of coherently diffracting Al matrix domains rather than the conventional metallographic grain size. This decrease in crystallite size

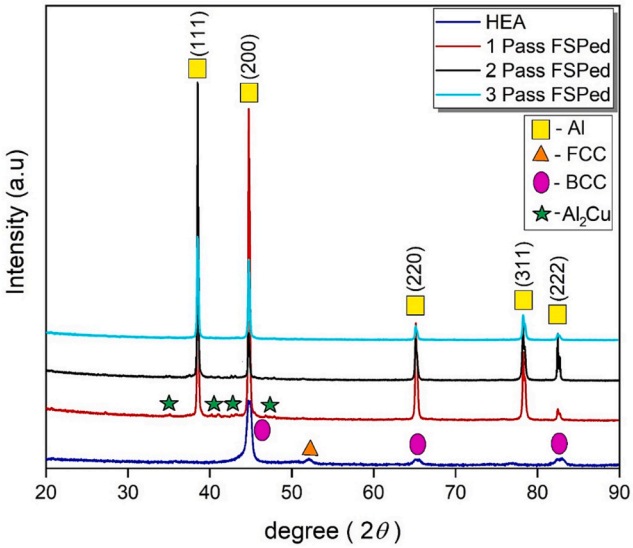

Fig. 5. XRD patterns of Al2024-HEA composites according to the number of passes.

Table 1
XRD-derived crystallite size (DP), microstrain (ε), dislocation density (δ), and d-spacing values of the FSPed samples with different pass numbers.

Sample Code	The crystalline size of the material 'nm' (Debye Scherrer)	Micro strain (ε, 10^{-3})	Dislocation density (δ)	D-spacing
1 Pass FSPed	45,22	1,91	$4{,}89\times10^{-4}$ nm^{-2}	1,635 Å
2 Pass FSPed	17,37	19,64	$3{,}31\times10^{-3}$ nm^{-2}	1,631 Å
3 Pass FSPed	14,35	27,79	$4{,}85\times10^{-3}$ nm^{-2}	1,626 Å

Table 2
Strength and elongation values of the base and MMC samples.

Condition	Tensile Strength (MPa)	Uniform Elongation (mm)
Base	188 ± 10	3 ± 0.5
1 Pass FSPed MMC	205 ± 9	2.8 ± 0.4
2 Pass FSPed MMC	234 ± 11	3.3 ± 0.4
3 Pass FSPed MMC	246 ± 8	3.6 ± 0.3

contributes to XRD peak broadening, as smaller coherently diffracting domains generally yield broader diffraction peaks. Microstrain and dislocation density values, however, increased significantly with the number of passes. For example, while microstrain was 1.91×10^{-3} in one pass, it reached 27.79×10^{-3} in three passes; similarly, dislocation density increased from 4.89×10^{-4} to 4.85×10^{-3}. This increased strain and dislocation density within the lattice causes the XRD peaks to broaden and appear lower-peaked, as well as to cause small shifts in their positions [64]. Indeed, the d-spacing values given in Table 1 appear to decrease slightly as the number of passes increases (from 1.635 Å in one pass to 1.626 Å in three passes). This decrease indicates a decrease in the Al lattice parameter, which may be due to internal stresses induced by increased microstrain or to the increased solubility of smaller atoms, such as Cu, into the Al matrix through multiple FSPs. Consequently, the reduction in crystallite size and the increase in microstrain/dislocation lead to a broadening and decreasing intensity of peaks in the XRD pattern, confirming the deformation-refined structure of the material.

Another important effect of increasing the number of passes is the gradual weakening of the XRD signatures of the Al_2Cu intermetallic phase present in the Al2024 alloy, disappearing completely in the high-

pass process (Fig. 5). While some faint peaks belonging to the Al_2Cu phase can be observed after a single pass of FSP, the characteristic peaks of this phase cannot be distinguished in the XRD pattern after a double-pass and, especially, a triple-pass process. This can be explained by the intense thermomechanical treatment applied by FSP dissolving the Al_2Cu (θ) phase into the aluminum matrix and homogenizing the structure. The high temperature and severe plastic deformation occurring during multiple passes cause Al_2Cu particles to break into small fragments and diffuse into the matrix, effectively dispersing Cu in solid solution within the Al. As a result, the peaks of this phase disappear in XRD because there is no longer a distinct Al_2Cu phase. The dissolution of the Al_2Cu intermetallic phase is a positive development for the composite; the removal of this brittle and corrosion-prone phase can allow for a more homogeneous distribution of Cu in the matrix, improving mechanical toughness and corrosion resistance. Furthermore, the supersaturated solid solution resulting from Cu dissolution within the matrix can improve the overall performance of the composite by providing a more homogeneous hardening mechanism rather than precipitation hardening [65].

On the other hand, some additional peaks observed in the spectrum indicate unique phases of the Fe-Ni-Cu-Cr-Al HEA added as reinforcement. This HEA reinforcement material is known to have a dual-phase microstructure, FCC and BCC, as reported in the literature. In the present composites, the HEA related reflections observed after FSP suggest that the reinforcement retained its identifiable crystalline features within the AA2024 matrix. A semi-quantitative comparison based on the relative peak areas of the visible HEA-related reflections showed no obvious change in the FCC/BCC phase balance with increasing FSP pass number. This indicates that the HEA reinforcement largely retained its dual-phase structure during FSP. However, the broadening and slight intensity variation of these peaks suggest lattice distortion and defect accumulation caused by severe plastic deformation rather than a distinct phase transformation. Some HEA peaks disappeared in the composite structure because they were almost identical to the Al peaks and the HEA reinforcement ratio was around 5%.

3.2. Hardness

Fig. 6 shows the Brinell hardness (HBN) values of MMCs produced using the base Al2024 alloy with high entropy alloy (HEA) additives and various number of FSP passes. The error bars represent the standard deviation of at least three measurements taken from different locations across the FSP stir zone. As can be seen, the hardness values show a significant and continuous increase with the increase in the number of FSP passes. In fact, while the hardness of the base Al2024 sample was 155 HBN, this value increased to 172 HBN in the MMC produced with one pass of FSP, to 217 HBN in the MMC produced with two passes of FSP, and to the highest value of 258 HBN in the MMC produced with three passes of FSP.

This increase in hardness values with increasing pass count is primarily due to the more homogeneous distribution of HEA particles within the matrix Al2024 phase. As can be seen in the microstructure images, as the number of passes increases, the HEA reinforcements distribute more homogeneously within the matrix phase, and clustering decreases significantly. This homogeneous distribution of reinforcing elements facilitates load transfer and enables the hard particles to resist deformation more effectively. This results in a stronger mechanical interlock between the matrix and reinforcement phase, particularly in MMCs produced with 2 and 3 passes of FSP, limiting local plastic deformation and significantly increasing hardness. Furthermore, the increased pass count also reduces void formation at the particle/matrix interfaces and improves interfacial integrity. Additionally, multiple FSP applications cause the HEA particles to break into smaller particles, thus increasing the total surface area.

3.3. Strength and elongation

The stress–strain curves of HEA reinforced MMCs produced by applying 1, 2, and 3 passes of FSP with the base Al2024 sample and the strength and elongation values obtained from these curves are shown in Fig. 7 and Table 2, respectively. The mechanical values in Table 2 are given as mean ± standard deviation based on at least three tensile tests, while Fig. 7 presents representative stress–strain curves for each condition. As can be seen, the base Al2024 alloy exhibits a tensile strength of 188 MPa, while this value increased to 205 MPa in MMC formed by applying 1 pass FSP. When the number of FSP passes applied during MMC formation was increased to 2, the tensile test showed a significant increase, reaching 234 MPa, while the tensile strength continued to increase in MMC formed with 3-passes of FSP, reaching 246 MPa. Although some scatter was observed in the tensile results, the standard deviations remained within an acceptable range for FSPed aluminum-based composites, where local microstructural heterogeneity may influence the fracture response. This increase in strength values following increased passes is mainly related to the increasingly homogeneous distribution of HEA particles within the matrix. As the number of passes increased, the tendency for the reinforcement phase to aggregate decreased, particle–matrix interactions strengthened, and load-carrying capacity became more effective, resulting in a significant upward trend in strength values. Furthermore, HEA particles are known to provide an effective barrier to dislocation motion. It is also believed that the increased homogeneity of HEA particles with increasing number of passes plays a more effective role in preventing dislocation motion, contributing to the increase in strength values.

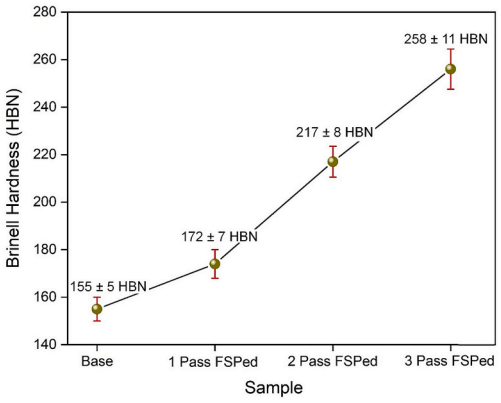

Fig. 6. Hardness measurement values taken from the base and MMC samples.

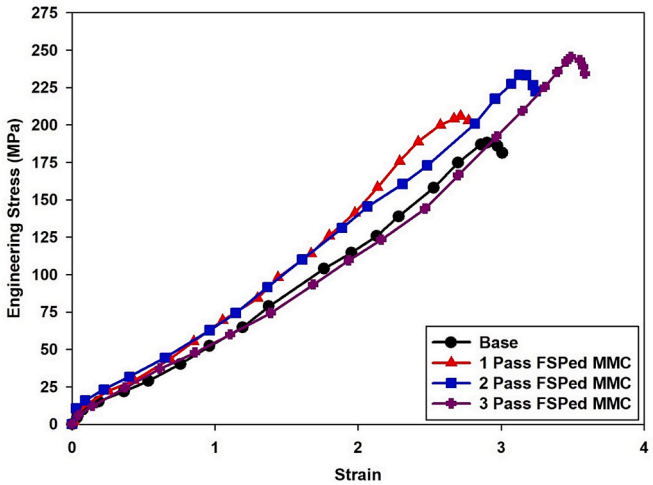

Fig. 7. Stress–strain curves of the base and MMC samples.

Examination of uniform elongation values revealed that the elongation rate in the base sample decreased slightly in the MMC produced by applying 1 pass of FSP, but began to increase when the number of passes was increased to 2 or 3. This decrease in elongation after 1 pass can be explained by the inability of the HEA particles to fully integrate into the matrix, leaving behind partial clusters and local heterogeneities. Such structural irregularities cause local stress concentrations during plastic deformation, increasing the tendency for crack initiation and limiting the elongation capacity. This interpretation is also consistent with the tensile fracture observations, where the 1-pass sample exhibited relatively less uniform dimple morphology and locally connected crack paths around clustered reinforcement regions. The increasing trend in elongation in the MMC produced by applying 2 and 3 passes of FSP indicates that the HEA particles are more homogeneously distributed, allowing for a more balanced stress transfer during deformation, thus preserving ductile behavior in the matrix. This result suggests that the improvement in elongation is not governed only by the presence of reinforcement particles, but also by the strength–ductility balance established through their more homogeneous distribution; this interpretation is consistent with previous findings on 2024 aluminum alloys showing that deformation and fatigue-related behavior are strongly affected by the balance between tensile properties and microstructural deformation mechanisms [66–68]. Furthermore, the reduction in particle size and improved interface quality with multiple passes slows crack propagation and contributes to the material's longer durability under deformation. In particular, the more homogeneous and finer dimple-like fracture features observed after 2 and 3 passes indicate a more stable ductile fracture response, which explains the recovery and subsequent improvement in elongation compared with the base alloy.

3.4. Wear properties

Fig. 8 illustrates the evolution of the coefficient of friction (CoF) with increasing reciprocating sliding cycles for the commercial AA2024 alloy and its composites reinforced with 10 wt% high-entropy alloy (HEA) particles, incorporated through one, two, and three passes of FSP. The base AA2024 alloy (blue curve) exhibits the highest coefficient of friction (CoF), initially increasing to around 0.75–0.80 within the first few hundred cycles. It then shows a gradual decreasing trend as the test progresses, reaching the range of 0.40–0.50 by around 3500 cycles, and maintains this level until the end of the test. The initial decrease in the coefficient of friction (COF) corresponds to the running-in stage, during which surface asperities are progressively smoothed, leading to surface conformity and a rapid increase in the real contact area. Simultaneously, a stable tribolayer is formed on the contact surface, which reduces direct metal–metal interaction and contributes to the observed decrease in COF. During this transient running-in period, noticeable fluctuations in the COF are observed due to the evolving contact conditions; however, these fluctuations gradually diminish as the system transitions into the steady-state wear regime. Such behavior is commonly reported for aluminum-based MMCs and explains the transient friction response observed in the early sliding cycles [4].

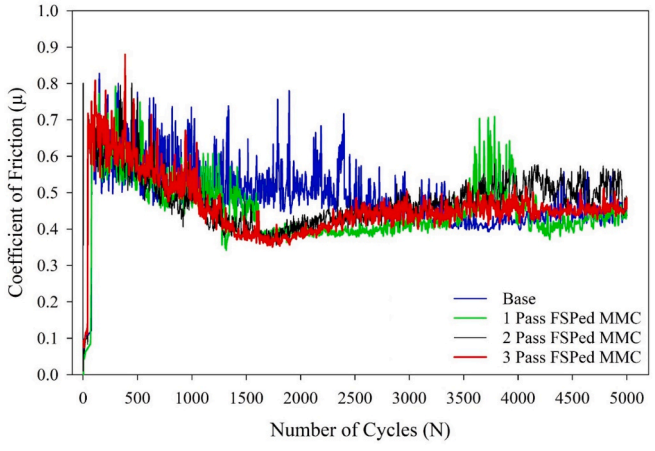

Fig. 8. Variation of the friction coefficients of the samples as a function of the number of reciprocating cycles.

Although the overall trend remains similar to the base material, a slight reduction and more stable behavior in the CoF is observed in the composite subjected to a single pass of FSP (green curve in Fig. 8), in which hard HEA particles were incorporated into the surface layer, as compared to the base alloy. The faster stabilization of the coefficient of friction observed in the HEA-reinforced Al–MMC compared to the unreinforced alloy can be primarily attributed to the accelerated formation of a stable friction film and the modification of the real contact conditions at the sliding interface. The presence of HEA particles increases the surface hardness and load-bearing capacity, thereby suppressing severe plastic deformation of surface asperities during the early sliding cycles. However, as the test progresses toward its final stages, the stable CoF trend observed between cycles 1500 and 3500 begins to deteriorate, leading to renewed instability. This behavior can be seen clearly between 3500 and 4200 cycles. This late-stage fluctuation in friction coefficient can be attributed to the insufficient homogeneity of HEA particle distribution within the matrix after a single FSP pass. Microstructural observations reveal the presence of partially mixed or locally clustered HEA particles regions in the one-pass specimen (Fig. 3), which are likely to induce localized variations in surface hardness and contact conditions during sliding. This non-uniformity may cause inconsistent shear resistance at the interface, which may result in CoF variability during the sliding.

Increasing the number of FSP passes to 2 and 3 (represented by the black and red curves, respectively) enhances the distribution of HEA particles within the microstructure, as illustrated in Fig. 3. Although this improved distribution does not reduce the coefficient of friction (CoF) values more, it contributes to a more stable CoF following the running-in period compared to the composite processed with a single FSP pass. This indicates that the main effect of repeated FSP is not only reducing friction but also stabilizing the sliding interface by improving load sharing between the AA2024 matrix and the HEA particles. In summary, HEA addition via FSP and additional FSP passes on it improve microstructural uniformity, which results in long-term stability in the CoF of the sample and can enhance the tribological performance of the MMCs sample.

The SEM images presented in Fig. 9 offer a detailed visualization of the wear tracks and wear mechanisms of the HEA-reinforced MMCs, highlighting the transition from fragmented layers to specific microscopic features induced by the incorporation of HEA particles and the progressive increase in FSP passes. For all samples (Fig. 9 a–l), the surface is dominated by clear signs of adhesive wear, resulting from the plastic deformation of the surface. However, the wear mechanism should be considered as a combined adhesive tribolayer controlled process rather than purely adhesive wear, since the fragmented surface layers, debris transfer, and counterface material adhesion indicate repeated formation and breakdown of tribofilms during sliding. Extensive metal transfer between the interaction surfaces and a fragmented tribolayer caused by deep adhesion cracks indicate the a notable sign of adhesive wear and severe plastic deformation for the unreinforced alloy (Fig. 9 a–c). The worn debris generated after the fragmentation of the tribolayer either detaches from the sliding interface, thereby accelerating material loss, or are transferred onto the counterface and subsequently re-transferred back onto the specimen surface, contributing to the cyclic reformation of the unstable tribofilm. These unstable and poorly adhered tribofilms are prone to early delamination under repeated sliding stresses. This morphological instability of the worn surface, characterized by poor tribolayer adherence and heterogeneous wear features, is consistent with the pronounced fluctuations in the friction coefficient observed in the base sample (Fig. 8). With the addition of 10 wt% HEA particles via a single FSP pass (images d–f), a

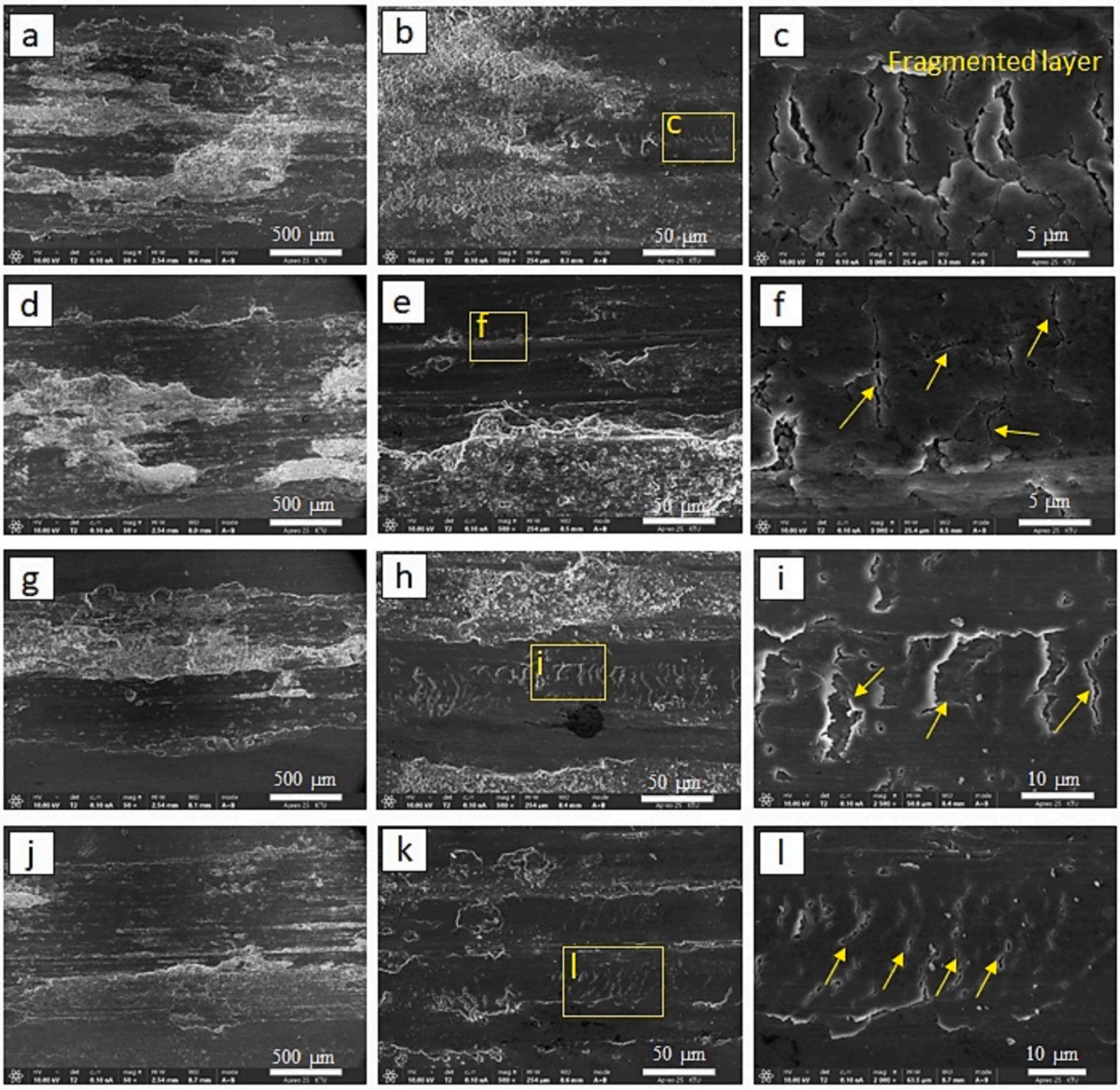

Fig. 9. SEM micrographs showing the appearance of worn surfaces of tested samples: (a-c) based, (d-f) 1 pass-FSPed MMC sample, (g-i) 2 Pass FSPed MMC sample and (j-l) 3 pass FSPed MMC sample.

limited change was observed on the surface morphology. This can be attributed to the presence of HEA powders in the structure of the 1-pass FSPed MMC sample, as the hard HEA reinforcements contribute to the partial stabilization of the tribolayer by acting as micro-scale load-bearing elements, minimizing localized plastic deformation and delaying tribolayer fragmentation. However, the presence of non-uniform particle distribution (Fig. 3) results in heterogeneous regions where the tribolayer stability varies. This partial stabilization corresponds well with the transient observed in the friction coefficient, which later deteriorates due to localized film breakdown. On the other hand, increasing the number of FSP passes (Fig. 9 (g–i) for two passes and Fig. 9 (j–l) for three passes) markedly changed the worn surface morphology by enhancing the HEA particle distribution within the microstructure. This homogenization enhances the formation of a more coherent and continuous tribofilm, evident by the reduced size and number of adhesion cracks. Although the thickness and composition of the tribolayer were not quantified, the SEM observations show a clear qualitative transition from unstable fragmented layers in the base and 1 pass samples to a more compact and continuous worn surface in the 3 pass sample. The tribological surface of the 3-pass FSPed MMC sample appears more compact and resistant to mechanical disruption, which is showing a more stable tribofilm that sustains consistent shear resistance and minimizes dynamic fluctuations in friction coefficient (Fig. 8).

The tribological performance of AA2024-HEA composites was also systematically investigated through wear debris analysis and counterface ball surface characterization. The presence of coarse, plate-like wear debris (Fig. 10 (a)) and significant adhesive material on the counterface ball (Fig. 10 (e and f)) indicate that the wear process of the base AA2024 alloy is primarily driven by adhesion-type mechanisms, along with severe plastic deformation and unstable tribolayer formation. Incorporation of 10 wt% HEA particles via a single FSP pass (Fig. 10. (b,g and h)) resulted in moderately refined wear debris and reduced adhesive transfer, suggesting partial stabilization of the tribo-interface. With the increasing number of FSP passes, a more uniform distribution of HEA particles within the matrix and improved stability of the tribolayer and increased hardness of the structure led to a gradual refinement in the morphology of the wear debris (Fig. 10 (c, d)) and a noticeable reduction in material transfer to the counterface (Fig. 10 (i–l)). This indicates that

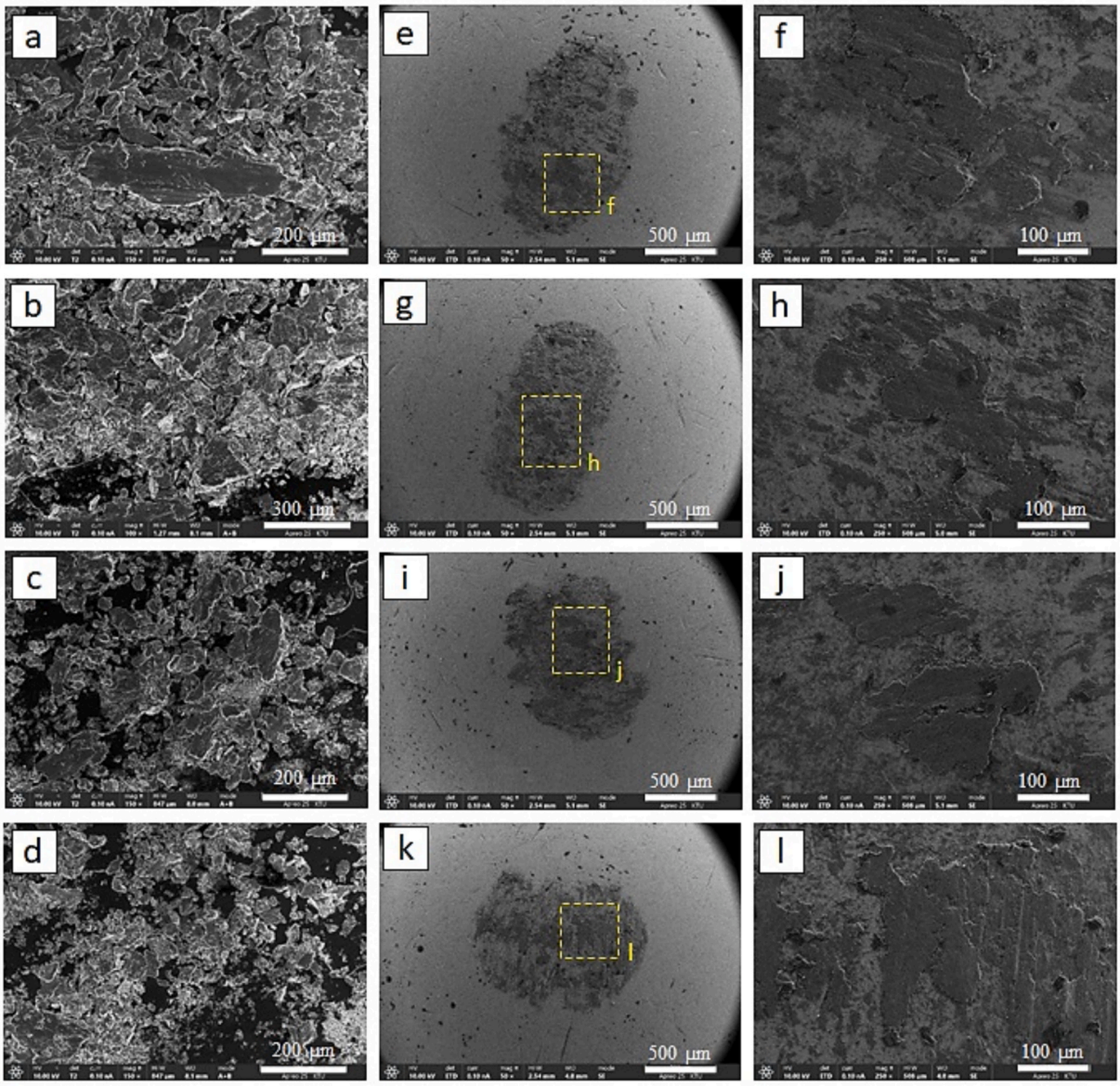

Fig. 10. SEM images illustrating the collected wear debris and the worn surfaces of the counterface ball for: (a, e, f) the base alloy, (b, g, h) the MMC subjected to 1 FSP pass, (c, i, j) 2 passes, and (d, k, l) 3 passes.

well-dispersed HEA particles act as load-bearing sites during sliding, while the refined and more stable wear debris contributes to the formation of a compact tribolayer rather than causing severe third-body abrasion. In this regard, Fe and Cr containing HEA particles may contribute to the load-bearing capacity and surface stability due to their relatively hard and oxidation-resistant character, whereas Ni may support tribofilm stability during repeated sliding. Cu containing regions may also assist local shear accommodation; however, this contribution is considered secondary compared with the dominant effect of particle dispersion and hardness improvement.

Fig. 11 shows the two-dimensional topographic views (2D) of the worn surfaces of the investigated samples. These images offer critical insight into the severity and uniformity of surface wear. The surface of the base AA2024 alloy reveals deep grooves, high roughness, and severe surface deformation. This irregular morphology is indicative of localized material detachment, intensive plastic deformation and high fluctuations in the CoF during dry sliding. A slight improvement in surface topography is observed after the incorporation of HEA particles via a single FSP pass. However, the surface still exhibits non-uniform features and localized rough zones. These results are in good agreement with previous findings on the heterogeneous HEA distribution in the 1-pass sample, which leads to localized differences in load-bearing capacity and tribolayer stability. The worn surface becomes noticeably more homogeneous, with reduced groove depth and smoother features following the 2-pass FSP. However, the 3-pass FSPed MMC sample has the smoothest surface morphology characterized by minimal surface roughness and highly uniform wear features. The roughness analysis obtained from the wear-track profiles also supports this trend, showing a gradual decrease in Ra and Rz values with increasing FSP pass number. Although detailed groove depth, width, and spacing measurements were not performed, the 2D topography and roughness profiles provide comparative evidence for reduced wear track severity with increasing pass number. This improvement can be associated with the presence of a stable and adherent surface film, resulting from the formation of a homogeneous microstructure. The consistent distribution of HEA particles effectively suppresses localized plastic deformation, thereby contributing to long-term wear stability.

Fig. 12 illustrates the volumetric wear rates of each sample under

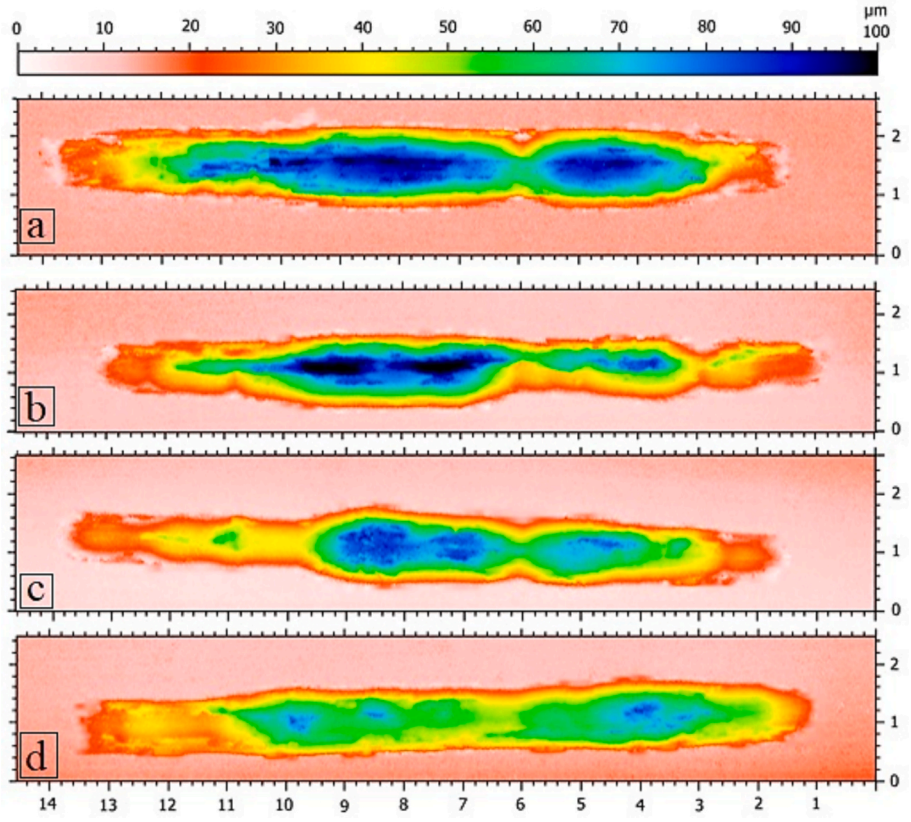

Fig. 11. 2D topographic images of the worn surfaces of the tested samples: (a) base, (b) 1-pass FSPed MMC, (c) 2-pass FSPed MMC, and (d) 3-pass FSPed MMC.

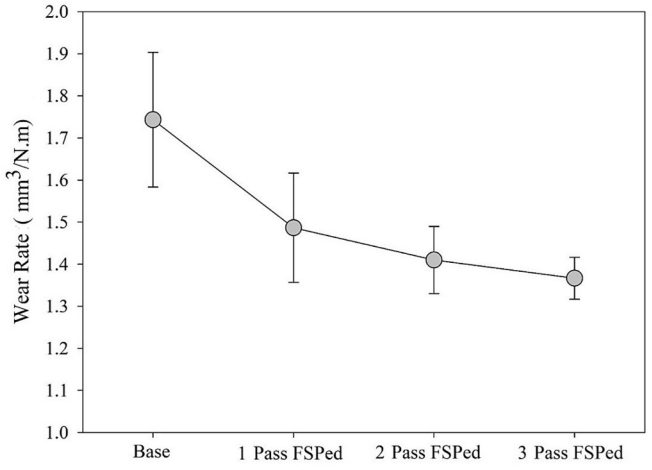

Fig. 12. Volumetric wear rates ($mm^3/(N{\cdot}m)$) of MMC samples under identical sliding conditions.

equivalent test conditions. The base sample shows the highest volumetric wear rate, confirming its poor tribological behavior. The absence of hard reinforcing particles in the structure contributes to the observation of more severe plastic deformation, which, combined with poor tribolayer integrity, results in significant material loss dominated by adhesive wear. The addition of HEA particles through 1-pass FSP, provided a sample that registered a reduced wear rate compared with the base alloy; however, the improvement in wear resistance was marginal, which is likely due to non-uniform particle distribution and break down of the tribolayer as shown previously in the CoF analysis and SEM images. The two-pass FSP exhibited less wear volume that can be attributed to better particle distribution and also harder matrix. A more homogenous surface topography, with a continuous, adherent tribolayer has provided the wear resistance performance in this sample. The lowest volumetric wear rate was achieved by the 3-pass FSPed MMC sample and can be attributed to the cumulative benefits of HEA reinforcement and repeated passes of FSP. This demonstrates the importance of microstructural homogeneity and surface stability on wear performance. Therefore, the improvement in wear resistance with increasing pass number can be interpreted as a gradual transition from severe adhesive wear with unstable tribolayer breakdown toward a milder wear regime controlled by improved particle distribution, enhanced load bearing capacity, and more stable tribofilm formation. The minimal wear volume correlates strongly with the most stable friction coefficient behavior, the smoothest worn surface topography, and the most compact tribofilm structure, as discussed in earlier sections.

3.5. Corrosion Behaviour

Fig. 13 and Table 3 show the potentiodynamic polarization curves and electrochemical corrosion data for MMCs fabricated with HEA reinforcement using the base Al2024 alloy and various FSP passes. The obtained data indicate that the MMCs exhibit better corrosion resistance than the base structure. In fact, the corrosion potential (Ecorr) of the base sample was measured as − 703 mV, the corrosion current density (Icorr) as 6.94 µA, and the corresponding corrosion rate as 14.79 mpy, while in the MMC treated with one pass of FSP, Ecorr decreased to − 661 mV, Icorr to 5.43 µA, and the corrosion rate to 10.42 mpy. In MMC formed by applying two passes of FSP, Ecorr was − 592 mV, Icorr was 3.22 µA and the corrosion rate decreased to 6.54 mpy, and in MMC formed by applying 3 passes of FSP, the corrosion resistance values were further improved and Ecorr increased to − 548 mV, Icorr decreased to 1.36 µA and the corrosion rate decreased to 3.11 mpy.

A significant increase in corrosion resistance was observed in MMCs formed by adding HEA particles to an aluminum matrix compared to the

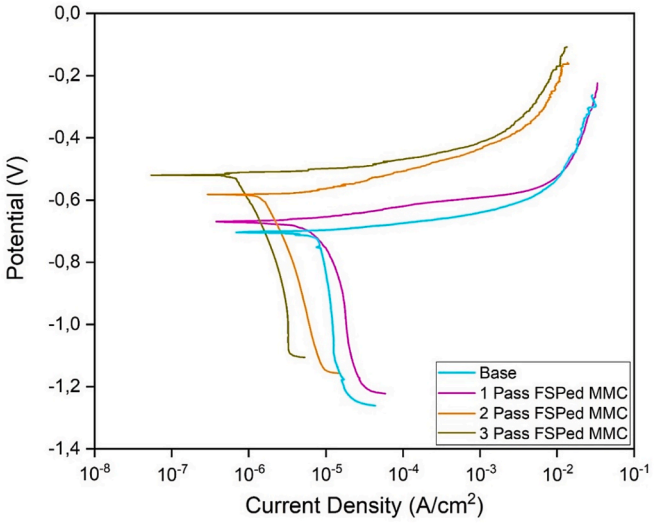

Fig. 13. Potentiodynamic polarization curves of the base and MMC samples.

Table 3
Electrochemical values of samples.

Condition	E_{corr} (mV)	I_{corr} (μA)	Corrosion Rate(mpy)
Base	−703	6.94	14.79
1 Pass FSPed MMC	−661	5.43	10.42
2 Pass FSPed MMC	−592	3.22	6.54
3 Pass FSPed MMC	−548	1.36	3.11

base alloy. This improvement is due to the positive effects of the HEA's chemical composition and the interaction between the particles and the matrix on corrosion behavior. The Cr and Ni elements in the HEA can contribute to the improved electrochemical response by promoting the stability of surface oxide species in corrosive environments. Cr containing oxides are commonly associated with improved resistance against localized corrosion, while Ni can support passive film stability and reduce electrochemical reaction kinetics. The improved polarization response also suggests that Cr- and Ni-containing surface oxides may contribute to the formation of a more protective passive film on the composite surface. Furthermore, when HEA particles are added to the matrix, residual compressive stresses are generated at the interface due to the difference in thermal expansion with the aluminum matrix. These stresses act as a mechanical barrier, preventing pit formation on the surface. The presence of the particles contributes to load transfer, making the structure more robust at the microscale and limiting the formation of weak areas where corrosion can propagate. In addition, the XRD results showed a reduction of the Al2Cu phase after FSP, which may also contribute to corrosion improvement by decreasing micro-galvanic coupling sites within the AA2024 matrix. As a result, the HEA additive increases corrosion resistance by providing chemical passivation thanks to the elements it contains and by reducing the corrosion rate and current density thanks to its microstructural barrier effects.

On the other hand, it was observed that the corrosion resistance of MMCs improved further with increasing the number of passes. This is due to the more homogeneous distribution of HEA particles within the matrix as a result of the increasing number of passes. SEM images reveal that the HEA particles become much more homogeneous within the matrix with increasing number of passes. This homogeneous distribution reduces the potential differences between the anode–cathode regions at the microscale, limiting the formation of galvanic cells and reducing the risk of localized corrosion. At the same time, homogeneous distribution reduces surface discontinuities and microporosity, thus limiting the movement of corrosive solutions. Post-corrosion surface observations also indicated that the base alloy exhibited more pronounced localized attack, whereas the multi-pass FSPed composites showed fewer and less severe corrosion pits. Furthermore, the homogeneous distribution of elements that contribute to passivation, such as Cr and Ni, supports the formation of more effective and stable passive films, resulting in lower corrosion current density.

4. Conclusions

In this study, AA2024/HEA MMCs were fabricated by incorporating FeNiCrAlCu high entropy alloy particles into the AA2024 alloy through FSP with different pass numbers, namely 1, 2, and 3 passes. The produced MMCs were compared with the base AA2024 alloy in terms of microstructural characteristics, mechanical properties, wear behavior, and corrosion resistance. The main findings obtained from the experimental analyses are summarized as follows:

1- The application of multiple passes allowed the HEA reinforcement particles to be distributed more homogeneously within the matrix. The 3-pass FSPed composite exhibited the most uniform microstructure among the processed samples.

2- Hardness showed a progressive increase with increasing FSP pass number, reaching 172 HBN after 1 pass, 217 HBN after 2 passes, and 258 HBN after 3 passes, compared to 155 HBN for the base AA2024 alloy.

3- Tensile strength increased from 188 MPa in the base AA2024 alloy to 205 MPa in the first pass, 234 MPa in the second pass, and 246 MPa in the third pass. The uniform elongation also increased to 3.6 ± 0.3 mm in the 3-pass FSPed composite, indicating that the improved particle distribution contributed to a better strength ductility balance.

4- Wear resistance improved with the HEA reinforcement and multiple passes, with the lowest wear volume loss in the three-pass application. The 3-pass FSPed composite showed the lowest volumetric wear rate and the most stable friction response, mainly due to enhanced microstructural homogeneity and improved tribolayer stability.

5- Corrosion resistance was also markedly enhanced. The corrosion rate decreased from 14.79 mpy for the base alloy to 10.42, 6.54, and 3.11 mpy after 1, 2, and 3 FSP passes, respectively, confirming the beneficial effect of multi-pass processing on electrochemical stability.

6- Overall, multi-pass FSP proved to be an effective route for enhancing the mechanical, tribological, and corrosion performance of AA2024/HEA MMCs by improving particle dispersion, interfacial integrity, and microstructural homogeneity.

Ethical approval

The authors declare that the research was conducted according to ethical standards. This article does not contain any studies with human or animal subjects.

7. Consent to participate

No external participants have contributed to the work discussed in this manuscript.

8. Consent for publication

The authors give their full consent to the editor to publish this article if accepted. The authors confirm that AI or AI-assisted technologies were not used in the writing process.

CRediT authorship contribution statement

Harun Yanar: Writing – original draft, Methodology, Investigation. **Dursun Murat Sekban:** Writing – original draft, Project administration, Data curation. **Serdar Ozkaya:** Writing – original draft, Investigation, Data curation. **Abdullah Hasan Karabacak:** Writing – original draft, Resources, Conceptualization. **Semih Mahmut Aktarer:** Writing – original draft, Formal analysis, Conceptualization. **Abdulkadir Coskun:**

Writing – review & editing, Visualization, Data curation. **Abdelouahed Tounsi:** Writing – review & editing. **Murat Yaylacı:** Writing – review & editing, Supervision.

Funding

This study has been supported by the Recep Tayyip Erdoğan University Development Foundation (Grant number: 02026002004091).

Declaration of competing interest

The authors declare that they have no known competing financial interests or personal relationships that could have appeared to influence the work reported in this paper.

Data availability

The data that support the findings of this study are available on request from the authors.

References

[1] M.S.K.K.Y. Nartu, P. Agrawal, Additive manufacturing of metal matrix composites, Mater Design 252 (2025) 113609.
[2] E.D. Yalçın, A. Çanakçı, H. Çuvalcı, T. Varol, A.H. Karabacak, The effect of boron nitride (h-BN) and silicon carbide (SiC) on the microstructure and wear behavior of ZA40/SiC/h-BN hybrid composites processed by hot pressing, Kovove Materialy-Metallic Materials 61 (4) (2023) 257–266.
[3] A.H. Karabacak, A. Çanakçı, S. Özkaya, S.A. Tunç, O. Güler, M. Çelebi, Effect of AlCrCuFeNi high entropy alloy reinforcements with and without B4C on powder characteristic, mechanical and wear properties of AA5083 metal-metal composites, J. Alloy. Compd. 1008 (2024) 176627.
[4] D.M. Sekban, S. Ozkaya, H. Yanar, A.H. Karabacak, S.M. Aktarer, A. Coskun, Effect of High-Entropy Alloy Amount on Microstructural and Mechanical Properties of Metal Matrix Composites Fabricated via Friction Stir Processing, Adv. Eng. Mater. 27 (2025) 2500724.
[5] A.H. Karabacak, A. Canakci, S. Özkaya, S.A. Tunç, Z.A. Çevik, E.D. Yalçın, The effects of different types and ratios of reinforcement, and machining processes on the machinability of Al2024 alloy nanocomposites, J. Compos. Mater. 57 (18) (2023) 2811–2827.
[6] S. Bahl, Fiber reinforced metal matrix composites - a review, Materials Today: Proceedings 39 (2021) 317-323.
[7] B. Singh, I. Kumar, K.K. Saxena, K.A. Mohammed, M. Ijaz Khan, S. Ben Moussa, S. Shukhratovich Abdullaev, A future prospects and current scenario of aluminium metal matrix composites characteristics, Alex. Eng. J. 76 (2023) 1–17.
[8] D.M. Sekban, Impact of 316L Stainless Steel on Microstructural and Mechanical Properties of AA5083/316L Metal Matrix Composites, Jom-Us 77 (4) (2025) 1969–1978.
[9] G. Bernard, V. Pejchal, O. Sereda, R.E. Logé, In-situ fabrication of Ti-TiCx metal matrix composite by laser powder bed fusion with enhanced elastic modulus and superior ductility, Mater Design 248 (2024) 113499.
[10] U. Çalıgülü, M.V. Kaçmış, A.H. Karabacak, A. Çanakçı, S. Özkaya, Investigation of corrosion resistance and impact performance properties of Al2O3/SiC-doped aluminium-based composites, Bull. Mater. Sci. 46 (3) (2023) 156.
[11] O. Mypati, J. Panzer, J.A. Robles-Linares, S. Zan, Z. Liao, D. Axinte, Modelling and experimental study of laser-assisted milling of fibre reinforced SiC/Ti-6Al-4V metal matrix composite, Mater Design 237 (2024) 112552.
[12] S. Gajević, S. Miladinović, O. Güler, S. Özkaya, B. Stojanović, Optimization of Dry Sliding Wear in Hot-pressed Al/B4C Metal Matrix Composites using Taguchi Method and ANN, Materials 17 (16) (2024) 4056.
[13] A. Kumar, V.P. Singh, R.C. Singh, R. Chaudhary, D. Kumar, A.-H.-I. Mourad, A review of aluminum metal matrix composites: fabrication route, reinforcements, microstructural, mechanical, and corrosion properties, J. Mater. Sci. 59 (7) (2024) 2644–2711.
[14] H. Singh, G. Singh Brar, H. Kumar, V. Aggarwal, A review on metal matrix composite for automobile applications, Materials Today: Proceedings 43 (2021) 320-325.
[15] P. Maurya, N. Kota, J. Gibmeier, A. Wanner, S. Roy, Review on study of internal load transfer in metal matrix composites using diffraction techniques, Mater. Sci. Eng. A 840 (2022) 142973.
[16] K.K. Sadhu, N. Mandal, R.R. Sahoo, SiC/graphene reinforced aluminum metal matrix composites prepared by powder metallurgy: a review, J. Manuf. Process. 91 (2023) 10–43.
[17] A. Graboś, P. Rutkowski, J. Huebner, P. Nieroda, D. Kata, S. Hayashi, Thermal properties of Inconel 625-NbC metal matrix composites (MMC), Mater Design 224 (2022) 111399.
[18] M. Chinababu, E. Bhaskar Rao, K. Sivaprasad, Fabrication, microstructure, and mechanical properties of Al-based metal matrix-TiB2 -HEA hybrid composite, J. Alloy. Compd. 947 (2023) 169700.
[19] S.A.A. Alem, M.H. Sabzvand, P. Govahi, P. Poormehrabi, M. Hasanzadeh Azar, S. Salehi Siouki, R. Rashidi, S. Angizi, S. Bagherifard, Advancing the next generation of high-performance metal matrix composites through metal particle reinforcement, Adv. Compos. Hybrid Mater. 8 (1) (2024) 3.
[20] S. Salifu, P.A. Olubambi, Microstructural and nanoindentation study of spark plasma sintered high entropy alloy reinforced aluminium matrix composites, J. Alloy. Compd. 999 (2024) 175021.
[21] S. Salifu, P.A. Olubambi, L. Teffo, Phase stability and microstructural properties of high entropy alloy reinforced aluminium matrix composites consolidated via spark plasma sintering, Heliyon 10 (2) (2024).
[22] V. Pandey, R. Seetharam, H. Chelladurai, A comprehensive review: Discussed the effect of high-entropy alloys as reinforcement on metal matrix composite properties, fabrication techniques, and applications, J. Alloy. Compd. 1002 (2024) 175095.
[23] X. An, F. Li, L. Kan, W. Zhang, J. Wang, X. Jin, Y. Wang, J. Li, H. Zhu, W. Qi, W. Wei, W. Sun, High entropy alloy particle reinforced 6061 aluminum matrix composites: an investigation of mechanical strength and thermoelectric properties, J. Alloy. Compd. 1010 (2025) 177424.
[24] S.A. Kareem, J.U. Anaele, E.O. Aikulola, U.S. Anamu, A. Koko, M.O. Bodunrin, K. K. Alaneme, Aluminium matrix composites reinforced with high entropy alloys: a comprehensive review on interfacial reactions, mechanical, corrosion, and tribological characteristics, J. Mater. Res. Technol. 30 (2024) 8161–8186.
[25] S. Salifu, P.A. Olubambi, High entropy alloy reinforced lightweight metal matrix composites: a review of the fundamentals, fabrication, properties, and prospects, Mater. Today Sustainability 32 (2025) 101216.
[26] Z.Y. Ma, Friction Stir Processing Technology: a Review, Metall. Mater. Trans. A 39 (3) (2008) 642–658.
[27] R.S. Mishra, P.S. De, N. Kumar, Friction Stir Processing, in: R.S. Mishra, P.S. De, N. Kumar (Eds.), Friction Stir Welding and Processing: Science and Engineering, Springer International Publishing, Cham, 2014, pp. 259–296.
[28] K. Li, X. Liu, Y. Zhao, Research Status and Prospect of Friction Stir Processing Technology, Coatings 9 (2) (2019) 129.
[29] D.M. Sekban, E. Uzun Yaylacı, M.E. Özdemir, Ş. Öztürk, M. Yaylacı, S.K. Panda, Formability behavior of AH-32 shipbuilding steel strengthened by friction stir process, Theor. Appl. Fract. Mech. 132 (2024) 104485.
[30] S.M. Aktarer, D.M. Sekban, O. Saray, T. Kucukomeroglu, Z.Y. Ma, G. Purcek, Effect of two-pass friction stir processing on the microstructure and mechanical properties of as-cast binary Al–12Si alloy, Mater. Sci. Eng. A 636 (2015) 311–319.
[31] M. Hajian, A. Abdollah-zadeh, S.S. Rezaei-Nejad, H. Assadi, S.M.M. Hadavi, K. Chung, M. Shokouhimehr, Microstructure and mechanical properties of friction stir processed AISI 316L stainless steel, Mater Design 67 (2015) 82–94.
[32] H.S. Grewal, H.S. Arora, H. Singh, A. Agrawal, Surface modification of hydroturbine steel using friction stir processing, Appl. Surf. Sci. 268 (2013) 547–555.
[33] Z.Y. Ma, S.R. Sharma, R.S. Mishra, Effect of friction stir processing on the microstructure of cast A356 aluminum, Mater. Sci. Eng. A 433 (1) (2006) 269–278.
[34] H. Zhao, Q. Pan, Q. Qin, Y. Wu, X. Su, Effect of the processing parameters of friction stir processing on the microstructure and mechanical properties of 6063 aluminum alloy, Mater. Sci. Eng. A 751 (2019) 70–79.
[35] K. Surekha, A. Els-Botes, Development of high strength, high conductivity copper by friction stir processing, Mater Design 32 (2) (2011) 911–916.
[36] M. Ebrahimi, M.A. Par, Twenty-year uninterrupted endeavor of friction stir processing by focusing on copper and its alloys, J. Alloy. Compd. 781 (2019) 1074–1090.
[37] W. Wang, P. Han, P. Peng, T. Zhang, Q. Liu, S.-N. Yuan, L.-Y. Huang, H.-L. Yu, K. Qiao, K.-S. Wang, Friction Stir Processing of Magnesium Alloys: a Review, Acta Metallurgica Sinica (english Letters) 33 (1) (2020) 43–57.
[38] B.M. Darras, M.K. Khraisheh, F.K. Abu-Farha, M.A. Omar, Friction stir processing of commercial AZ31 magnesium alloy, J Mater Process Tech 191 (1) (2007) 77–81.
[39] Z. Ding, Q. Fan, L. Wang, A Review on Friction Stir Processing of Titanium Alloy: Characterization, Method, Microstructure, Properties, Metall. Mater. Trans. B 50 (5) (2019) 2134–2162.
[40] F. Cao, T. Sun, J. Hu, W. Hou, G. Huang, Y. Shen, N. Ma, P. Geng, W. Hu, X. Qu, Enhanced mechanical and anticorrosion properties in cryogenic friction stir processed duplex stainless steel, Mater Design 225 (2023) 111492.
[41] N. Kumar, R.S. Mishra, N.B. Dahotre, R.E. Brennan, K.J. Doherty, K.C. Cho, Effect of friction stir processing on microstructure and mechanical properties of laser-processed Mg4Y3Nd alloy, Mater Design 110 (2016) 663–675.
[42] S.M. Aktarer, T. Kucukomeroglu, D.M. Sekban, E.U. Yaylaci, M. Yaylaci, M. E. Ozdemir, I. Mirzaloglu, Analysis of the changes in microstructure, mechanical, and contact properties of multi-pass friction stir processed DP800 steel, Adv. Nano Res. (2025) 253–264.
[43] S.C. Kundurti, A. Sharma, P. Tambe, A. Kumar, Fabrication of surface metal matrix composites for structural applications using friction stir processing – A review, Materials Today: Proceedings 56 (2022) 1468-1477.
[44] B.R. Sunil, G.P.K. Reddy, H. Patle, R. Dumpala, Magnesium based surface metal matrix composites by friction stir processing, J. Magnesium Alloys 4 (1) (2016) 52–61.
[45] S. Sahraeinejad, H. Izadi, M. Haghshenas, A.P. Gerlich, Fabrication of metal matrix composites by friction stir processing with different Particles and processing parameters, Mater. Sci. Eng. A 626 (2015) 505–513.
[46] S. Singla, P. Sagar, A. Handa, A.S. Kang, Recent advances in Magnesium-based Metal Matrix Surface Composites developed via Friction Stir Processing Route—An Overview, Metall. Microstruct. Anal. 12 (3) (2023) 385–400.

[47] D.K. Sharma, V. Badheka, V. Patel, G. Upadhyay, Recent Developments in Hybrid Surface Metal Matrix Composites Produced by Friction Stir Processing: a Review, J. Tribol. 143 (5) (2021).
[48] D. Ghanbari, M.K. Asgharani, K. Amini, Investigating the effect of passes number on microstructural and mechanical properties of the Al2024/SiC composite produced by friction stir processing, Mechanics 21 (6) (2015) 430–436.
[49] E. Moustafa, Effect of Multi-Pass Friction Stir Processing on Mechanical Properties for AA2024/Al2O3 Nanocomposites, Materials 10 (9) (2017) 1053.
[50] S.S. Abdelhady, R.E. Elbadawi, S.H. Zoalfakar, Evaluation the effect of multi-pass friction stir processing on the wear, mechanical properties, and microstructure of the AA1050/ZrO2 surface nanocomposite, Discover Applied Sciences 6 (10) (2024) 498.
[51] C. Wang, X. Zhu, Z. Wang, X. Xiao, K. Zhang, C. Jiang, J. Liu, Microstructure and mechanical properties of Al/(Cu-Ni) hybrid composite via ball milling and friction stir processing, J. Alloy. Compd. 1037 (2025) 182289.
[52] P. Karmiris-Obratański, I.G. Papantoniou, B. Leszczyńska-Madej, Microstructure, mechanical and tribological properties of AA5083-TiO2 nanocomposite by multi-pass friction stir processing, Arch. Civ. Mech. Eng. 24 (4) (2024) 209.
[53] M. Zhang, M. Paidar, O.O. Ojo, S. Mehrez, S. Narayanasamy, A.M. Zain, V. Mohanavel, Impact of multiple FSP passes on structure, mechanical, tribological and corrosion behaviors of AA6061/316 stainless-steel reinforced Al matrix composites, Surf. Coat. Technol. 447 (2022) 128801.
[54] M. Nikzad-Dinan, R. Jamaati, H. Jamshidi Aval, Enhanced microstructure, strength, and wear resistance of AA2024-AlB2 composites via multi-pass friction stir processing, J. Mater. Res. Technol. 36 (2025) 4293–4307.
[55] S. Guo, C.T. Liu, Phase stability in high entropy alloys: Formation of solid-solution phase or amorphous phase, Prog. Nat. Sci.: Mater. Int. 21 (6) (2011) 433–446.
[56] D.B. Miracle, O.N. Senkov, A critical review of high entropy alloys and related concepts, Acta Mater. 122 (2017) 448–511.
[57] V. Rubtsov, A. Chumaevskii, A. Gusarova, E. Knyazhev, D. Gurianov, A. Zykova, T. Kalashnikova, A. Cheremnov, N. Savchenko, A. Vorontsov, V. Utyaganova, E. Kolubaev, S. Tarasov, Macro- and Microstructure of In Situ Composites Prepared by Friction Stir Processing of AA5056 Admixed with Copper Powders, Materials 16 (3) (2023) 1070.
[58] K. Qiao, T. Zhang, K. Wang, S. Yuan, L. Wang, S. Chen, Y. Wang, K. Xue, W. Wang, Effect of multi-pass friction stir processing on the microstructure evolution and corrosion behavior of ZrO2/AZ31 magnesium matrix composite, J. Mater. Res. Technol. 18 (2022) 1166–1179.
[59] J. Li, Y. Li, F. Wang, X. Meng, L. Wan, Z. Dong, Y. Huang, Friction stir processing of high-entropy alloy reinforced aluminum matrix composites for mechanical properties enhancement, Mater. Sci. Eng. A 792 (2020) 139755.
[60] N. Li, C.-L. Jia, Z.-W. Wang, L.-H. Wu, D.-R. Ni, Z.-K. Li, H.-M. Fu, P. Xue, B.-L. Xiao, Z.-Y. Ma, Y. Shao, Y.-L. Chang, Achieving a High-Strength CoCrFeNiCu High-Entropy Alloy with an Ultrafine-Grained Structure via Friction Stir Processing, Acta Metallurgica Sinica (english Letters) 33 (7) (2020) 947–956.
[61] B.S. Gong, Z.J. Zhang, H.W. Wang, R. Liu, H.Z. Liu, G. Purcek, M. Demirtas, H. Yanar, Z.F. Zhang, Improving the fatigue limit of FSW6061 Al alloy welded joints by surface spinning rolling, Int. J. Fatigue 200 (2025) 109119.
[62] C. Wang, X. Zhu, K. Zhang, X. Xiao, C. Jiang, J. Zhang, C. Lv, Study on the microstructure and mechanical properties of Al matrix composites reinforced with nano Ni via friction stir processing, J. Mater. Res. Technol. 36 (2025) 2284–2296.
[63] B.S. Gong, Z.J. Zhang, H.W. Wang, R. Liu, H.Z. Liu, H. Wang, G. Purcek, M. Demirtas, H. Yanar, Z.F. Zhang, A novel surface strengthening technique for enhancing fatigue properties of 6061 Al alloy, Int. J. Fatigue 198 (2025) 109000.
[64] S. Prakrathi, M. Ravikumar, K.R. Udupa, K. Udaya Bhat, Fabrication of Hybrid Surface Composite through Friction Stir Processing and its Impression Creep Behaviour, International Scholarly Research Notices 2013 (1) (2013) 541762.
[65] A. Lalpour, M. Mosallaee, A. Ashrafi, A. Zargaran, Microstructural Evolution in the Friction Stir Processed AA2024, Mater. Trans. 64 (8) (2023) 1894–1901.
[66] F. Liu, F. Zhu, W. Yang, Q. Wang, Y. Tu, Improved mechanical properties of 2024 aluminum alloys by electric pulse assisted rolling and subsequent aging, Mater Design 254 (2025) 114053.
[67] B.S. Gong, Z.J. Zhang, J.P. Hou, R. Liu, Q.Q. Duan, H.W. Wang, X.G. Wang, H. Z. Liu, H. Wang, G. Purcek, M. Demirtas, H. Yanar, Z.F. Zhang, Effects of aging state on the low-cycle fatigue properties of, aluminum alloy, J. Mater. Res. Technol. 29 (2024) (2024) 2448–2457.
[68] Y. Zhang, B. Gong, Z. Ba, L. Zhang, L. Zong, L. Jiang, Y. Zhu, W. Yang, Z. Jia, W. Sun, Simultaneous enhancement of mechanical and fatigue properties in 2xxx aluminum alloys via microstructural uniformity induced by cyclic plasticity, Sci. China Mater. (2026).